Results in Chemistry 18 (2025) 102891

Contents lists available at ScienceDirect

Results in Chemistry

journal homepage: www.sciencedirect.com/journal/results-in-chemistry

Acetaldehyde detection using nickel-incorporated WO_3 thin films prepared via spray pyrolysis

Roshini Xavier [a], Logu thirumalaisamy [b], Santhosh Nallakumar [a], Thangavel Ravikumar [a], Anju Thomas [a], Janani Arunachalam [a], Anand Sekar [c], Kalainathan Sivaperuman [a], G. Swati [a,*]

[a] Centre for Nanotechnology and Research, Vellore institute of technology, Vellore 632014, India
[b] Department of Physics, GTN Arts College (Affiliated to Madurai Kamaraj University), Dindigul 624001, India
[c] Department of science and humanities, Dhanalakshmi Srinivasan College of Engineering, Coimbatore - 641105, India

ARTICLE INFO

Keywords:
Tungsten oxide thin films
Spray pyrolysis technique
Chemi-resistive gas sensors
Acetaldehyde sensor

ABSTRACT

Acetaldehyde, a compound known for its cellular and genomic toxicity, poses a significant threat to both human health and environmental safety. This underscores the urgent need for cost-effective and highly sensitive sensors capable of detecting acetaldehyde at low concentrations. In this study, metal oxide semiconductor–based thin-film gas sensors were developed using pure and nickel-doped tungsten trioxide (WO_3). The thin films were fabricated via spray pyrolysis, a direct deposition technique that yielded crystalline monoclinic-phase WO_3 with a favourable surface morphology conducive to gas sensing. Among the samples, the 5 % Ni-doped WO_3 (WO_3:Ni-5) film exhibited the highest performance, delivering an impressive sensing response of 102.28 at room temperature. The enhanced response was attributed to the incorporation of Ni^{2+} ions, which induced the growth of nanorods within a fibrous, flower-like microstructure, thereby increasing the active surface area. Comprehensive characterisation confirmed that the sensor has good selectivity towards acetaldehyde (25 S), sensitivity (5 ppm), repeatability, humidity tolerance, and long-term stability, establishing its strong potential for practical acetaldehyde detection.

1. Introduction

The World Health Organization (WHO) estimates that indoor air pollution is responsible for approximately 4.2 million premature deaths annually, highlighting it as a critical yet often overlooked public health issue. In many developing countries, the use of solid fuels such as wood, coal, and dung for cooking and heating releases harmful pollutants into enclosed spaces. This issue is further compounded by indoor tobacco smoke, which contains numerous carcinogens; second-hand smoke alone is known to cause thousands of lung cancer-related deaths each year. While global efforts have led to noticeable improvements in outdoor air quality particularly in reducing pollutants like nitrogen dioxide (NO_2) and sulphur dioxide (SO_2) indoor air pollution remains inadequately addressed. In 2022 alone, indoor air pollution accounted for an estimated 3.2 million deaths. Additionally, commonly used household items such as cleaning agents, paints, adhesives, and synthetic furnishings release volatile organic compounds (VOCs) that further degrade indoor air quality [1–3].

VOCs are a major class of indoor air pollutants due to their ease of evaporation at room temperature and their prevalence in both natural and anthropogenic sources. Among these, acetaldehyde has emerged as a particularly hazardous compound. It is emitted from numerous indoor sources such as tobacco smoke, cooking emissions, and off-gassing from building materials and consumer products. Industrially, acetaldehyde is used as a precursor for acetic acid and in the manufacture of perfumes, paints, and food flavouring agents. At concentrations above 100 ppm, it gives off a strong, pungent odour, whereas at lower levels (below 50 ppm), it smells sweet and fruity. Despite its widespread use, acetaldehyde is classified as a probable human carcinogen, and its high volatility significantly increases the likelihood of inhalation exposure. To mitigate health risks, regulatory bodies such as the Occupational Safety and Health Administration (OSHA) have set an 8-h permissible exposure limit of 25 ppm. The European Flavour Association (EFFA, 2010) has also emphasized that chronic exposure to acetaldehyde can elevate cancer risk. These facts underline the urgent need for continuous and accurate monitoring of acetaldehyde in indoor environments [4–7].

* Corresponding author.
E-mail address: swati.g@vit.ac.in (G. Swati).

https://doi.org/10.1016/j.rechem.2025.102891
Received 1 September 2025; Accepted 14 November 2025
Available online 15 November 2025

To meet this demand, Chemi-resistive gas sensors have emerged as a promising technology for efficient VOC detection, particularly for compounds like acetaldehyde. These sensors are well-suited for real-time, on-site monitoring due to their low manufacturing cost, ease of miniaturization, compatibility with electronic devices, and resilience to environmental changes [8]. Chemi-resistive sensors detect gases by converting chemical interactions at the sensor's surface into measurable electrical signals. Among them, metal oxide semiconductor (MOS) sensors stand out for their high sensitivity, rapid response, and ability to detect low gas concentrations. Their application in detecting acetaldehyde at room temperature offers a practical and energy-efficient solution for addressing the growing challenge of indoor air pollution.

Transition metal oxides, in particular, offer enhanced sensing performance due to their narrow bandgap and variable oxidation states, which promote significant changes in electrical conductivity during gas interaction. Among these, oxides with d^0 (e.g., TiO_2, WO_3) and d^{10} (e.g., ZnO) electronic configurations have demonstrated especially high effectiveness in gas sensing applications, due to their favourable electronic structures and surface reactivity [9]. N-type metal oxide semiconductors are ideal for gas sensors due to their electron-dominated charge transport and Fermi level near the conduction band. Compared to p-type counterparts, they offer lower baseline resistance, simpler fabrication, and efficient operation at lower temperatures, making them highly suitable for sensor applications [10–13]. WO_3 is a robustly researched n-type semiconducting transition metal oxide material that exhibits excellent stability in oxidative and corrosive environments [14]. WO_3 is a great option for gas sensing applications because of its high sensitivity to both reducing and oxidising gases, as well as its long hole diffusion length and good electron mobility [15,16]. Its versatility and responsiveness to various gases highlight its potential for environmental and industrial monitoring [17]. Pure WO_3 typically operates at high temperatures and suffers from limited selectivity, as well as slow response and recovery times. However, doping WO_3 can introduce lattice defects, increase oxygen vacancy concentrations, modify the band gap, or introduce impurity levels within the band structure, all of which contribute to a marked improvement in its gas sensing performance [18,19]. Nickel (Ni) doping was specifically chosen to modify WO_3 based on its potential to enhance key gas-sensing parameters such as sensitivity, selectivity, and response/recovery time. Nickel oxide (NiO) is well-known for its high oxygen adsorption capacity compared to other metal oxides, making it an ideal material for chemical catalysts and gas sensors [20]. Nickel is one of the most favoured transition metal (TM) dopants for altering the optical and electrical characteristics of semiconductors [18]. According to Singkammo. et al., when combined with a SnO_2 sensor, a NiO p-type catalyst demonstrated a better sensing response, selectivity, and quicker reaction time towards sensing of volatile organic compounds [21,22]. This study has demonstrated that incorporating transition metals such as Ni into metal oxide semiconductors can lead to the formation of defect states that improve charge carrier mobility and gas sensing response. Hence, Ni was used as a potential dopant in WO_3 lattice. To optimise the concentration of Ni, WO_3 thin films with different concentration of Ni (0.01, 0.03, and 0.05 M) was prepared namely WNi-1, WNi-3, and WNi-5, respectively. To the best of the authors' knowledge, few reports exist on studies employing WO_3 thin film gas sensors operating at room temperature. We observed that Ni doping enhances the sensor performance under ambient conditions and lower detection limits (5 ppm) was also achieved in this study.

Present work discusses the development of an acetaldehyde gas sensor operable at room temperature using a single-step deposition technique. Inspired by the findings of Kuan Tian et al. [23], which demonstrated that WO_3/NiO bilayer gas sensors exhibit excellent sensitivity and response towards triethylamine (TEA) upon the incorporation of NiO, the present work explores the fabrication and performance of pure and nickel-incorporated WO_3 thin films. These films were synthesized via spray pyrolysis with the aim of achieving efficient acetaldehyde detection under ambient conditions. Comprehensive characterisation techniques, including X-ray diffraction (XRD), field emission scanning electron microscopy (FE-SEM), and X-ray photoelectron spectroscopy (XPS), were employed to investigate the correlation between the films' microstructural features and their gas-sensing performance. These analyses provided insight into how Ni incorporation influences crystallinity, surface morphology, and chemical states, ultimately contributing to enhanced sensing behaviour. Furthermore, both pure and Ni-doped WO_3 films were systematically analysed for their structural, optical, morphological, and gas-sensing properties, with all measurements conducted under ambient conditions at room temperature (28 °C).

2. Experimental details

2.1. Preparation of intrinsic and Ni-doped WO_3 thin films via spray pyrolysis

The synthesis process plays a key role in defining the microstructural characteristics, which have a greater influence on the performance of gas sensors. Spray pyrolysis, a cost-effective single-step technique, offers advantages over other deposition methods, including easy doping, moderate operating temperatures (100–500 °C), precise film thickness control, and compatibility with various substrates without requiring a vacuum. The spray deposition technique is employed to deposit both intrinsic WO_3 and nickel-doped WO_3, as illustrated in Fig. 1a. Tungstic acid (Sigma Aldrich 99 %) was added to a mixture of 20 mL ammonia solution and 40 mL deionized water. The precursor solution is stirred for 1 h at 80 °C until a clear solution is obtained. This clear solution of ammonium meta tungstate is sprayed onto the soda lime glass substrate (7 cm × 2.5 cm) to obtain a WO_3 thin film. While spraying, the substrate was maintained at 290 °C. Spray deposition was accomplished with an air-atomised spray gun. The precursor solution is sprayed using atmospheric air as a carrier gas with a moderate pressure ranging from 0.5 to 1.5 bar. The thin films were deposited at a substrate temperature of 290 °C using a spray gun positioned at a 45° angle. Ni-doped WO_3 thin films are developed by adding three different concentrations of Nickel (II) chloride hexahydrate ($NiCl_2.6H_2O$), diluted in 10 mL DI water, to the ammonium meta tungstate solution. The films that resulted from varying the nickel concentrations to 0.01, 0.03, and 0.05 M were dubbed WNi-1, WNi-3, and WNi-5, respectively. A thorough cleaning of the glass substrate is essential in order to guarantee the best possible adherence of the deposited material. The distance between the substrate and nozzle was fixed to be approximately 28 cm. The average flow rate of the precursor solution was ~1.37 mL/min. After 25 iterations of spray deposition cycles, the film was allowed to cool before being annealed for an hour at 500 °C (5 °C each minute). After that, the resultant films-WO_3, WNi-1, WNi-3, and WNi-5 were characterised using the necessary methods.

2.2. Characterisation

Studies using powder-X-ray diffraction were conducted in order to ascertain the nanostructures' crystal structure and crystallite size. Using Cu Kα radiation (λ = 1.5418 Å) at 30 kV and 20 mA, a Bruker diffractometer (D8 advanced) was employed. A step size of 0.02° and a scanning range of 20–40° were used. The thin-film optical absorption spectra were acquired using ultraviolet-visible spectroscopy (JASCO-650-PC); the wavelength range was kept between 300 and 800 nm. To analyse the surface roughness, atomic force microscopy (AFM) was utilized to obtain 2D and 3D topographic images of the thin films (Nano surf easy Scan 2), operated in contact mode. A field emission scanning electron microscope (FE-SEM, Zeiss Sigma LV 300 model) was employed to examine the morphology of the thin films. The volatile organic compounds at room temperature were measured using a specially designed gas sensing setup, which consists of a chamber with gas input and outlet and a lead wired to link the film. A Keithley (6517B) source meter is used

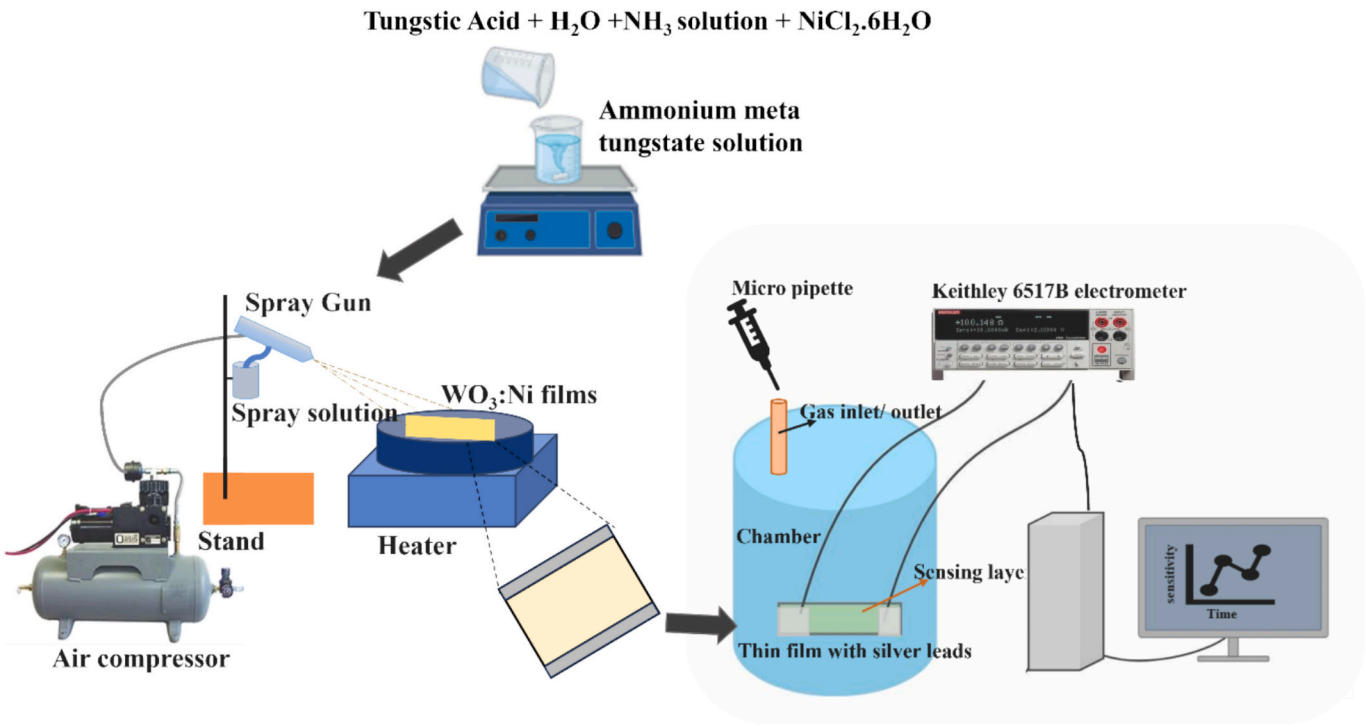

Fig. 1. Schematic representation of Ni-doped WO_3 thin film fabrication by spray pyrolysis and the gas-sensing measurement setup.

to measure resistance or current flow.

2.3. Gas sensing setup

A gas sensing unit was used to test the prepared thin film sensor. Point connections were created on the surface of the sensor, using silver paste and copper wire with negligible resistance. The dimensions of both electrodes were fixed to 1.5 cm × 1.5 cm. The two electrode connections were separated by a distance of 1 cm. Crocodile clips were used to secure a high-resistance electrometer to the sensors. A Keithley electrometer (6517B) and a PC setup were connected to the thin film sensor to analyse data in real-time. After which, the thin film was placed inside the sensing chamber, which is equipped with a vapour outlet and a gas inlet.

A 5 V operating voltage was applied to the thin film sensor, and the resulting current was monitored until a stable baseline was established. Due to an increasing need for room temperature gas sensors, the entire setup was kept at room temperature. The necessity for room temperature gas sensors can be attributed to various factors, including the high-power consumption and expenditure associated with microheaters. A schematic diagram of the gas sensing setup is shown in Fig. 1a. Using the following expression, the suggested concentration of the VOCs was calculated.

$$C_{(ppm)} = \frac{\delta \times V_\Gamma \times R \times T \times 10^6}{M \times P_b \times V_b} \quad (1)$$

where, δ is the density of target molecules, V_Γ is the volume of VOC purged into the chamber, R-gas concentration, T-absolute temperature, V_b- the volume of the chamber (L), P_b- chamber pressure (Pascal), M-molecular weight of VOC. The thin film-based sensor starts to react with gas molecules as soon as the gas is purged into the chamber [24]. A high-resistance electrometer measured the current change induced by the Chemi-resistive sensor surface. To return the baseline current to its original level, fresh air was introduced into the chamber after each measurement.

3. Results and discussions

3.1. X-ray diffraction (XRD)

Using the X-ray diffraction technique, the annealed samples were characterised for their structural properties, as shown in Fig. 2. The predominant peaks in the spectra are discernible at Bragg's angle 2Θ = 22.4°, 23.9°, 24.7°, 28.04°, 33.39°, 37.17°, 50.54° and 56.84° respectively. These correspond to the (002), (020), (200), (112), (022), (202), (400), and (124) reflections of WO_3 thin film. The peaks are well following (JCPDS Card no:01–072-1465) [25] of monoclinic phase with lattice parameters, a = 7.30 Å, b = 7.56 Å and c = 7.68 Å. In the WO_3 sample, (002) is the primary intensity peak. The incorporation of Ni into the WO_3 lattice can be rationalized based on ionic size compatibility and charge compensation effects. Although the substitution of Ni^{2+} for W^{6+}

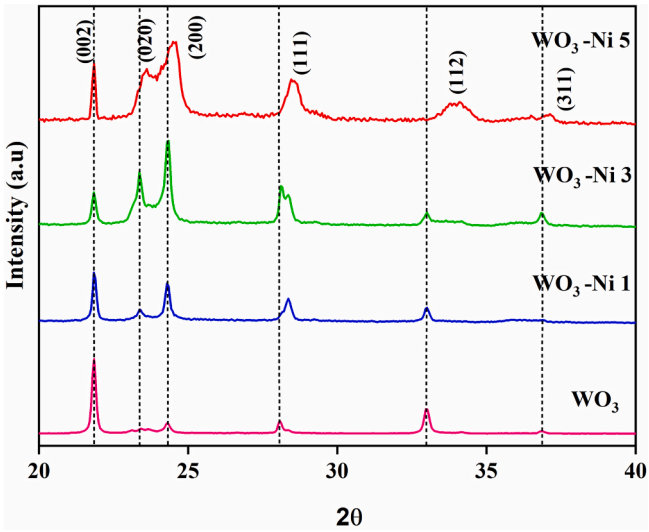

Fig. 2. X-ray diffraction pattern of the deposited thin films.

is not charge-neutral, the modest difference in their ionic radii ($Ni^{2+} \approx 0.69$ Å; $W^{6+} \approx 0.60$ Å) allows Ni to occupy octahedral sites with minimal lattice distortion. Charge neutrality is maintained through the formation of oxygen vacancies and partial reduction of tungsten to W^{5+}, as supported by XPS analysis. These oxygen vacancies are a common and energetically favourable mechanism in transition metal oxides, stabilizing Ni incorporation at low concentrations. At higher doping levels, Ni may also segregate locally or form NiO clusters, potentially introducing p–n type interfaces. The structural modifications align with the observed peak shifts and broadening in XRD patterns, thereby confirming the successful doping of Ni. [26–30]

It is noted that the intensity decreases with the introduction of nickel dopant. This change in intensity is attributed to the lattice distortion and strain induced by the substitution of W^{6+} ions with Ni^{2+} ions in the WO_3 lattice. The incorporation of Ni^{2+} in place of W^{6+} creates size and charge imbalance, which is compensated by the formation of oxygen vacancies and mixed W^{6+}/W^{5+} valence states to maintain charge neutrality. These structural distortions alter the lattice parameters and crystal orientation preference, leading to a change in the growth direction of crystallites from the (002) plane to the (200) plane. [31] Thus, the shift and intensity variation in the XRD peaks confirm successful Ni doping and the resulting modification of the WO_3 crystal structure. These microstructural changes are consistent with the FE-SEM images that show modified filamentous/rod growth when Ni is present. With increasing doping concentration, the crystallite size decreases from 44 nm to 24 nm. This occurs because dopant ions accumulate at the grain boundaries, raising the energy barrier for the diffusion of W^{6+} ions. This higher barrier restricts the crystal's growth and expansion [32]. The crystallite size, dislocation density and micro strain are listed in the following Table 1.

3.2. UV- visible spectroscopy

UV–visible absorption spectra and the optical band gap of pure and Ni-doped WO_3 thin films were investigated. Every sprayed film has notable absorption properties. The band gap of WO_3 was estimated using the Tauc plot eq. (2), as shown in Fig. 3b.

$$\alpha h\nu = A\,(h\nu - Eg)^2 \quad (2)$$

Tauc's equation relates the optical band gap (Eg), the minimum energy needed for an electron to move from the valence band to the conduction band. α is the absorption coefficient, $h\nu$ = Photon energy (eV), where h is Planck's constant and ν is frequency of incident light. The equation involves a temperature-independent constant (A). The band gap values for WO_3, WNi-1, WNi-3, and WNi-5 were determined to be 3.97 eV, 3.8 eV, 3.69 eV, and 3.61 eV, respectively. A decrease in band gap energy (E_g) is observed with increasing dopant concentration, as the optical band gap is influenced by dopant-induced modifications in the density of localized electronic states. This variation in band gap may also be attributed to the sp-d exchange interaction between band electrons and the localized d electrons of Ni ions.

In the case of absorbance spectra, a redshift is observed as the dopant concentration increases [33]. The absorbance peaks of the WO_3, WNi-1, WNi-3, and WNi-5 films were found to be 288, 298, 312, 315.7 nm, respectively in Fig. 3a.

Incorporation of Ni into the WO_3 lattice slightly modifies its electronic structure, leading to possible band-gap narrowing. The doping process generates oxygen vacancies, which introduce defect states between the valence and conduction bands, thereby reducing the band gap and improving electrical conductivity. With increasing Ni^{2+} concentration, oxygen vacancies and lattice distortions become more pronounced, generating defect-induced sub-band states that further decrease the optical band gap.

The consistent red shift observed in both absorption edge and band-gap energy confirms that Ni doping induces band-gap narrowing through the creation of defect states and electronic hybridization effects.

3.3. Atomic force microscopy (AFM)

The thin film topography was examined, and the surface roughness was measured using Nano surf easy Scan 2 in contact mode atomic force microscopy. The root mean square roughness was measured to be 896 nm, 952.8 nm, 1004.9 nm, and 1111.2 nm for WO_3, WNi-1, WNi-3, and WNi-5, respectively. As the dopant concentration increases, the surface roughness also upsurges, allowing more gas molecules to interact with the thin film surface through various adsorption sites. According to Fig. 4(a,b,d,e,g,h,j,k), 2D and 3D pictures of AFM, the spray-deposited samples were discovered to be densely packed, free of cracks, and rough on the surface. The microfibre patterns are illustrated in 2D AFM images. Spray pyrolysis involves several temperature-dependent processes affecting the aerosol, such as precipitation, chemical bond formation, nucleation, and diffusion. These processes contribute to the surface roughness of the film, enhancing its capacity to adsorb target molecules [4].

3.4. Field emission scanning electron microscopy (FE-SEM)

FE-SEM images of the deposited films are presented in Fig. 4(c, f, i, l). All the films have flower-like architecture with layers resembling petals encircling a pore-filled core.

The surface seems to have a roughness, which could help gas molecules adsorb and improve the sensitivity of the sensor [34]. The filamentous flower-like structures of the Ni-doped films seem to have nanorods [35,36] that are well-distributed throughout the thin film surface, which may enable a greater responsive surface area. The film's comparable morphologies, which include larger holes and a rough surface, aid in the adsorption of gas molecules [37]. The pure film appears to have some visible pores in the middle and fewer nanorods on the film surface. This appears to be more pronounced on Ni-doped films with more surface roughness. The fibre's network allows more gas molecules to penetrate between the layers, creating extended pathways for gas adsorption [34]. The roughness and fibrous structure of the films offer a superior surface-to-volume ratio, enhancing the interaction between the sensor surface and gas molecules [38]. The interaction of gas molecules with the film's surface plays a crucial role in determining the sensor's performance. Energy-dispersive X-ray Analysis (EDAX) was used to determine the elemental distribution within the samples. The results of this analysis are presented in Supplementary, and Fig. 3f, g, h shows the EDAX spectrum and mapping images of the WNI-5 film. The films consist of W, Ni, and O, with no unwanted peaks detected. The EDAX results for the doped samples indicate Ni weight percentages of 0.35 %, 0.44 %, and 0.89 % for WNi-1, WNi-2, and WNi-3, respectively. The atomic ratios of tungsten were 63.05 % for the pure sample, and 72.42 %, 78.49

Table 1
Average crystallite size, micro strain and dislocation density of the deposited WO_3 and Ni-doped WO_3 thin films.

Samples	Crystallite Size (nm)	Micro-Strain (x 10^{-3} lines $^{-2}$ m^4)	Dislocation Density δ (x 10^{14} m^2)	Lattice constant a (Å)	Lattice constant b (Å)	Lattice constant c (Å)	β (°)
WO_3	44	4.7	5.1	7.211	7.435	7.999	96.03
WNI-1	34	6.4	8.6	7.147	7.433	7.997	96.05
WNI-3	29	6.7	11.8	7.209	7.401	8.163	97.06
WNI-5	24	6.9	17.3	7.231	7.437	8.037	97.05

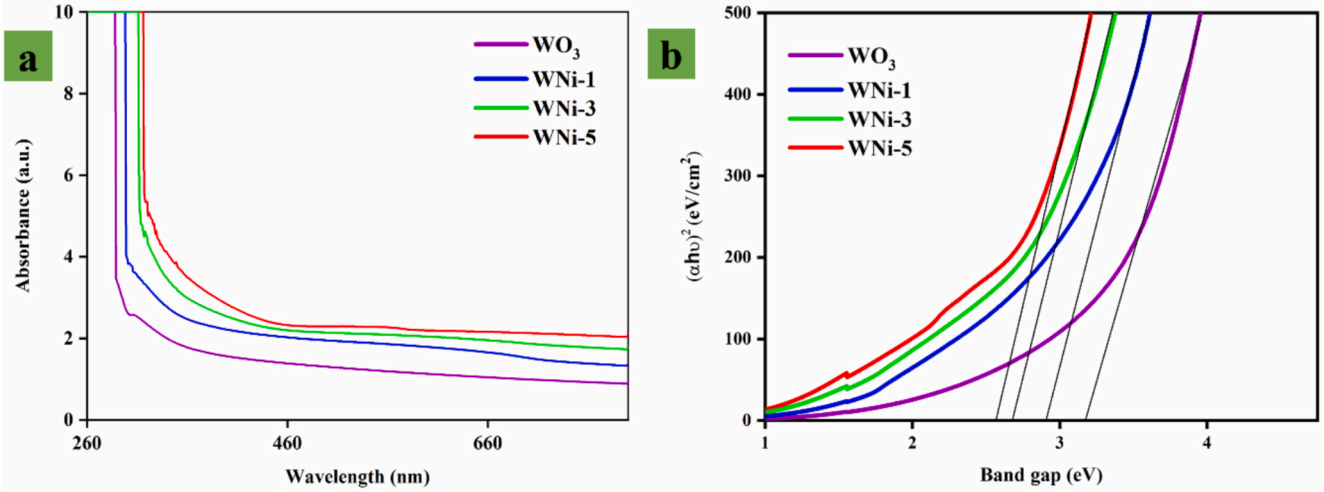

Fig. 3. (a)Absorption spectra of UV–Visible spectroscopy (b) Tauc plot from the UV–Visible spectroscopy of the deposited WO_3, WNi-1, WNi-3, WNi-5 samples.

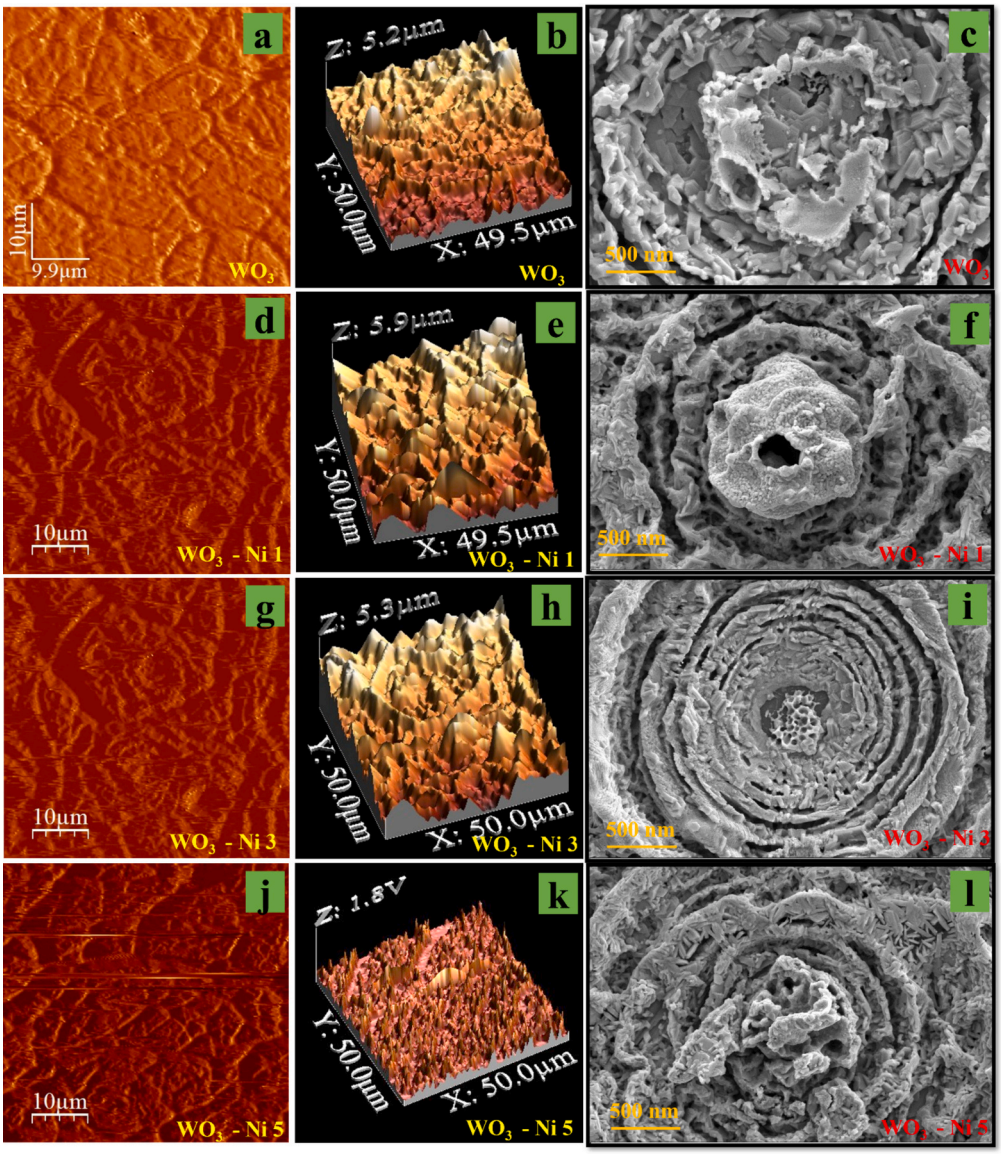

Fig. 4. 2D images (a, d, g, j) and 3D images (b, e, h, k) of the deposited film using atomic force microscopy and FE-SEM images (c, f, i, l) of deposited films.

%, and 69.62 % for WNi-1, WNi-2, and WNi-3, respectively as shown in EDAX spectra.

3.5. X-ray photoelectron spectroscopy (XPS)

To evaluate the chemical state of atoms within films, X-ray Photoelectron spectroscopy was carried out on nickel-doped WO_3 film (WNi-1) as shown in Fig. 5a of the XPS survey spectrum. The peaks at 35.5 eV ($W4f_{7/2}$) and 37 eV($W4f_{5/2}$) show the presence of W^{6+}, as shown in Fig. 5b [39]. The incorporation of Ni element into the host lattice is confirmed with its characteristic peaks at 857 eV corresponding to Ni $2P_{3/2}$ of Ni $^{2+}$ state and 870 eV corresponding to Ni $2P_{1/2}$,as shown in Fig. 5d [26,40]. The deconvoluted peak at 530.9 eV corresponds to the O1S spectrum of oxygen in Fig. 5c, indicating the presence of oxygen in WO_3 [41]. With BE standard adjustment, the computed binding energy of C—C is 284.8 eV, as shown in Fig. 5e, which shows a strong correlation with Vijayan et al [42]. This finding confirms that Ni ions have been successfully incorporated into the WO_3 crystal lattice. Nickel doping in the films substantially altered the gas-sensing behaviour of WO_3 by influencing the density of oxygen vacancies and the supply of oxygen ions on the WO_3 surface [29].

3.6. Gas sensing mechanism and studies

Various reducing gases, such as ethanol, 2-butanol, benzene, ammonia, acetone, and acetaldehyde, were utilized for the selectivity test at a 10-ppm concentration. Among all the other VOC gases evaluated for selectivity, the WO_3 thin film exhibited the highest sensing response towards acetaldehyde in terms of conductance (25.4), as illustrated in Fig. 6a for a 10-ppm concentration at a temperature of 28 °C.

Ensuring a stable baseline current in clean air is essential. Once a stable baseline current is established, a redox reaction between the gas molecules and the metal oxide semiconductor surface is expected upon exposure to the VOC test gas. The film's current changes as a result of the electrons being donated or accepted based on this reaction between the test gas and sensing material. Following each cycle of gas exposure, the baseline is re-established. One way of explaining the sensing process is that, in ambient circumstances, oxygen molecules adsorb onto the WO_3 sites on the surface, causing ionisation and the development of a

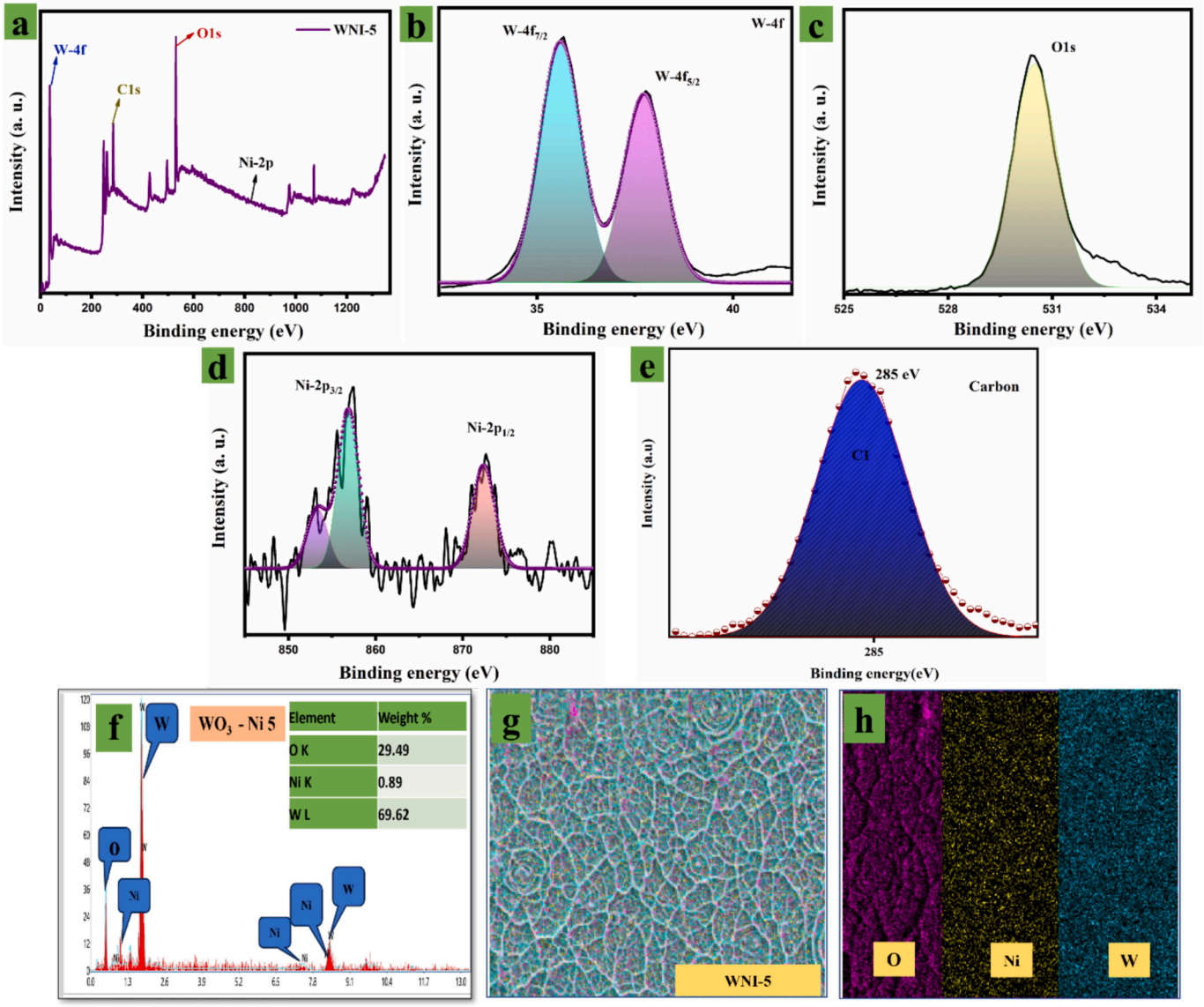

Fig. 5. (a) Survey spectrum, (b) Tungsten, (c) Oxygen peak, (d) Nickel, (e) Carbon peaks from X-ray photoelectron spectroscopy and (f) the EDAX spectrum and (g) and (h) EDAX mapping images of the deposited film WNI-5.

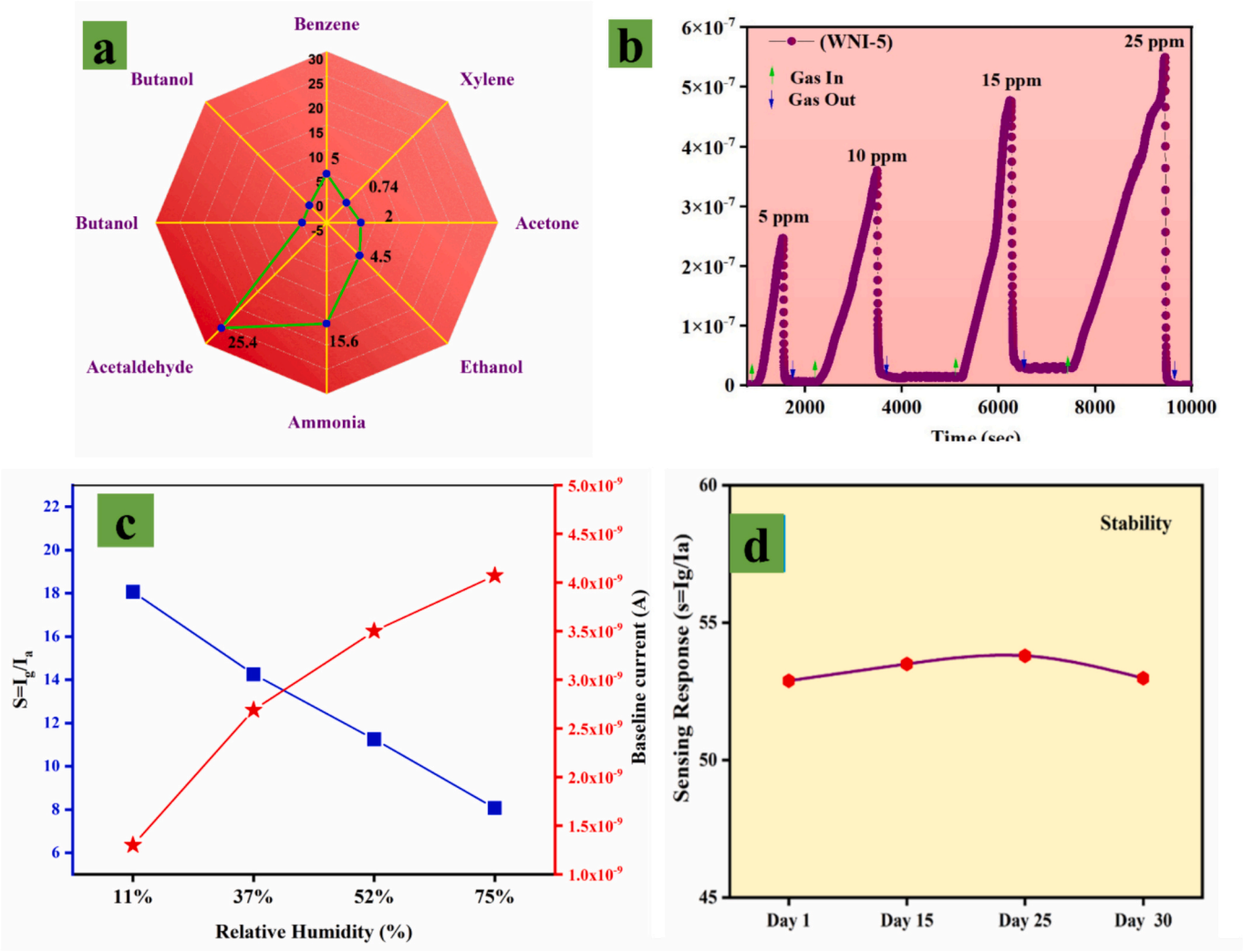

Fig. 6. The gas sensing (a) selectivity of the deposited WO_3 film, respectively, (b)Transient response curve of WNI-5 sample, (c)Relative humidity vs sensor response and relative humidity vs baseline current of WNi-5 and (d) stability.

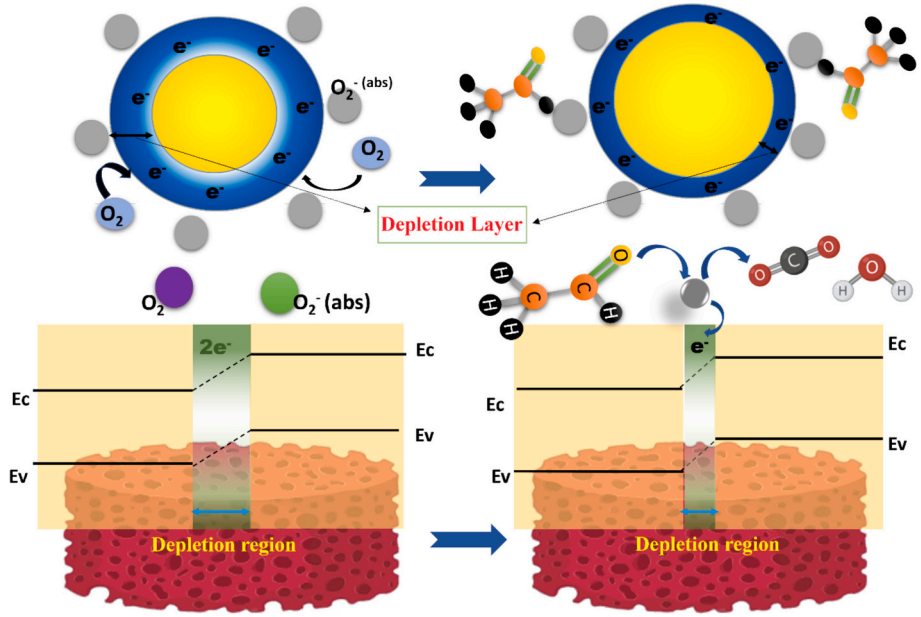

Fig. 7. Schematic representation of sensing mechanism.

depletion region. The reaction kinematics of the deposited film and the gas molecule is explained with eq. (3). Upon exposure of the deposited thin films to acetaldehyde gas, the reducing gas may interact with the ionic oxygen species,

$$O_2\ (\text{adsorbed}) + e^-\ (\text{material}) \rightarrow O_2^-\ (\text{adsorbed}) \quad (3)$$

$$2CH_3CHO + 5\ O_2^- \rightarrow 4CO_2 + 4H_2O + 5e^- \quad (4)$$

As a consequence of the reaction between O_2^- ions and acetaldehyde, CO_2, H_2O, and electrons are generated as by-products. The discharged electrons return to the conduction band. During the recovery process, acetaldehyde molecules detach from the film's surface. This leads to a wider depletion region, which ultimately causes the sensor's resistance to return to its original state [43]. A schematic diagram explaining the sensing mechanism with electron transition is shown in Fig. 7. The stability of the deposited films over 1–30 days was investigated and almost 97 % of the stability was achieved Fig. 6d. The repeatability of the gas sensor is a very important factor in determining the authenticity of the dynamic response value. The WNi-5 films show good repeatability as depicted in Supplementary.

Fig. 6b shows the dynamic sensing response of WO_3 and Ni-doped WO_3 thin films to acetaldehyde gas at concentrations ranging from 5 to 25 ppm. The porous WO_3 film showed a sensing response value of $I_{gas}/I_{air} = 52.78$ S for a 25-ppm concentration of acetaldehyde. For nickel-doped WO_3 films, the WNi-1's maximum response was found to be ($I_{gas}/I_{air} = 63.71$ S) at 25 ppm, and it appears that this value rises as the dopant concentration does. For WNi-3 ($I_{gas}/I_{air} = 83.56$ S) sensing response, and a maximum response value of ($I_{gas}/I_{air} = 102.28$ S) was reported for WNi-5 film. This follows the morphology and surface roughness of the films. Filamentous flower-like structures, along with increased surface roughness as the doping concentration augmented, the gas sensing response. From FE-SEM analysis, the WNi-5 film seems to have a rougher texture with a greater number of visible nanorods on the surface as compared to pristine WO_3 films, WNi-3 and WNi-1. For thin-film gas sensors, response and recovery times are crucial parameters. The response time is defined as the time required for the sensor to attain 90 % of its maximum signal upon gas exposure. The recovery time is measured as the time taken for the sensor signal to decrease to 10 % of its peak value after the gas is removed [44]. The highest sensing response of the deposited films was 102.28 S for a 10-ppm gas concentration. The response and recovery times of the deposited WNi-5 film are illustrated graphically in Supplementary. The response and recovery time of deposited film WNi-5 were found to be ~933 s and ~ 11 s, respectively.

The high density of surface states in nanocrystal structures, as observed in FE-SEM, significantly increases the reactivity of the sensor surface, enabling strong oxygen adsorption even at low temperatures. This enhanced oxygen adsorption broadens the depletion zone at the oxide surface, leading to greater upward band bending. Consequently, an inversion layer forms, shifting the Fermi level (E_F) below the intrinsic level (E_i) and replacing the conventional depletion layer typically induced by surface adsorption. These nanocrystals exhibit exceptional gas-sensing capabilities for both oxidising and reducing gases, even at low temperatures. The enhanced sensing performance can be attributed to their reduced surface area, which facilitates adsorption and oxygen ionosorption [29]. Some Ni ions can replace the W^{6+} ions in the lattice when Ni is doped with WO_3; others can even create a local p-n junction. The gas sensitivity and resistance of the sensor will be controlled by the resistance of these p-n junctions, rather than the Schottky barriers at the WO_3 grain boundaries. In the case of pure WO_3, when the sensor is exposed to air, oxygen molecules stick on the surface and capture electrons from the sensor material. This reduces the number of free-flowing electrons in the sensor. When Ni is added to WO_3, the resulting doped sensor material has a larger depletion layer, trapping more electrons and leading to higher resistance than pure WO_3. Electrons are released back into the sensor when reducing gas is introduced and reacts with the oxygen on the surface. The doped film's Ni ions act as a barrier to stop the electrons from recombining and vanishing. The proportion of p-n junctions to Schottky barriers in Ni^{2+}doped WO_3 films depends on the concentration and distribution of NiO within the material [45]. Thus, their p-n junction can adjust the work function and band bending, altering the height of the Schottky barrier and enhancing the sensing response [46,47]. A comparative Table 2 has been provided, summarizing the performance of existing Ni-doped WO_3-based gas sensor in terms of their sensing response and other key parameters. Among the studies reviewed, the present work highlights the acetaldehyde sensing performance of various gas sensor systems.

3.7. Relative humidity

The impact of the Relative humidity (RH) on the sensing capability of the WNi-5 film was tested. The sensors were exposed to 10 ppm CH_3CHO at relative humidity (RH) of 11 %, 32 %, 52 %, and 75 %. Relative humidity was maintained using saturated salt solutions (LiCl, $MgCl_2$, $Mg(NO_3)_2$, and NaCl, respectively within a test chamber. A hygrometer (HTC Instruments, HD-306) was used to monitor the RH values [12]. Fig. 6c shows a significant increase in the sensors' initial current with rising humidity (11 % to 75 %). This is probably due to the formation of a proton transfer layer as water molecules adsorb onto the sensor film, with subsequent water dissociation into H_3O^+ or H^+ ions increasing conductivity and current. Fig. 4c further illustrates the effect of decreasing humidity on sensor response. At low RH (11 %), water vapour might enhance CH_3CHO detection, possibly by facilitating the catalytic reaction and boosting the signal. However, higher RH correlates with decreased sensor response. This is likely because water molecules occupy active sensor sites, thereby hindering CH_3CHO adsorption. At higher RH, a dense water layer further impedes CH_3CHO adsorption, affecting both the WNi-5 film's response magnitude and its response/recovery times. The presence of hydroxyl groups reduces available reaction sites, limiting the acetaldehyde response. This effect is more prominent in WO_3, suggesting its greater reactivity with hydroxyl groups [51–53].

4. Conclusion

Tungsten trioxide (WO_3) and Ni-doped WO_3 thin films were successfully fabricated via spray pyrolysis and evaluated for acetaldehyde sensing at room temperature. Structural and morphological analyses revealed that Ni incorporation preserved the monoclinic crystal structure while reducing crystallite size, increasing surface roughness, and inducing oxygen vacancies, which collectively enhanced surface reactivity. WO_3, WNi-1, WNi-3, and WNi-5 were found to have band gap values of 3.97 eV, 3.8 eV, 3.69 eV, and 3.61 eV, respectively. For WO_3, WNi-1, WNi-3, and WNi-5, the corresponding root mean square roughness measurements were 896 nm, 952.8 nm, 1004.9 nm, and 1111.2 nm. Among the studied films, the 5 % Ni-doped sample (WNi-5) exhibited

Table 2
Comparison of Acetaldehyde sensing performance of various gas sensors.

Material	Operating temperature	Sensing response	Gas (concentration in ppm)	Reference
Co-In_2O_3	300 °C	0.85[a]	100	[48]
Ru-SnO_2/WO_3	300 °C	10[a]	100	[49]
Rh-SnO_2	350 °C	17.8[a]	40	[50]
NiO: WO_3 nanosheet heterojunction	250 °C	2184[b]	100	[30]
Ni doped WO_3	Room temperature	102.28[a]	25	**This work**

[a] $S = \frac{Ra}{Rg}$, [b] $S = \frac{(Ra - Rg)}{Ra} \times 100$.

the best performance, delivering an exceptionally high response of 102.28 S at 25 ppm acetaldehyde, superior to previously reported WO_3-based sensors. The sensor further demonstrated excellent selectivity towards acetaldehyde over other VOCs, along with a response (933 s), quick recovery (11 s), good repeatability, and stability across multiple cycles and varying humidity conditions. The observed filamentous, flower-shaped structures with rod-shaped clusters significantly contributed to enhanced gas adsorption and charge transfer, explaining the improved sensing behaviour. These findings highlight Ni doping as an effective strategy to tailor the structural and electronic properties of WO_3, thereby enabling high-performance gas sensors. Overall, spray-deposited Ni-doped WO_3 thin films emerge as promising candidates for low-cost, energy-efficient, and reliable acetaldehyde detection systems, with strong potential for integration into next-generation indoor air quality monitoring devices.

CRediT authorship contribution statement

Roshini Xavier: Writing – original draft, Visualization, Resources, Methodology, Data curation, Conceptualization. **Logu thirumalaisamy:** Writing – review & editing, Conceptualization. **Santhosh Nallakumar:** Writing – review & editing, Visualization, Investigation. **Thangavel Ravikumar:** Resources, Data curation. **Anju Thomas:** Methodology, Formal analysis, Data curation. **Janani Arunachalam:** Writing – review & editing, Resources. **Anand Sekar:** Writing – review & editing, Investigation, Formal analysis. **Kalainathan Sivaperuman:** Writing – review & editing, Supervision. **G. Swati:** Validation, Supervision, Resources, Funding acquisition.

Declaration of competing interest

The authors declare that they have no known competing financial interests or personal relationships that could have appeared to influence the work reported in this paper.

Acknowledgement

The authors would like to acknowledge the school of advanced science and centre for nanotechnology research at VIT for the facilities provided for the work.

Appendix A. Supplementary data

Supplementary data to this article can be found online at https://doi.org/10.1016/j.rechem.2025.102891.

Data availability

Data will be made available on request.

References

[1] A.C. Lewis, D. Jenkins, C.J.M. Whitty, Indoor air pollution: five ways to fight the hidden harms, Nature 614 (2023) 220–223.
[2] N. Singh, S. Agrawal, S. Jiwnani, D. Khosla, P.S. Malik, A. Mohan, P. Penumadu, K. T. Prasad, Lung Cancer in India, J. Thorac. Oncol. 16 (2021) 1250–1266, https://doi.org/10.1016/j.jtho.2021.02.004.
[3] I. Johansson, The Role of Volatile Organic Compounds in the Assessment of Indoor Air Quality, 1999.
[4] T. Ravikumar, L. Thirumalaisamy, K. Sivaperuman, Synergistic effect of rGO decoration on ZnFe2O4 nanorods for low concentration detection of ammonia at room temperature with high selectivity and response, Surf Interfaces 53 (2024) 105076, https://doi.org/10.1016/j.surfin.2024.105076.
[5] P. Wolkoff, VOC - sources, measurements, emisions, and the impact on indoor air quality, Indoor Air 3 (1995) 73.
[6] A. Mirzaei, H.W. Kim, S.S. Kim, Nanostructured Semiconducting Metal Oxide Gas Sensors for Acetaldehyde Detection, (2019) 1–16.
[7] A. Thomas, L. Thirumalaisamy, S. Madanagurusamy, K. Sivaperuman, Switching the selectivity of ZnO thin films for ultra-sensitive acetaldehyde gas sensors through co doping, Sens. Actuators B 401 (2024) 135043, https://doi.org/10.1016/j.snb.2023.135043.
[8] W. Gao, Y. Bai, X. Wang, H. Fu, P. Zhao, P. Zhu, J. Yu, Self-standing perylene diimide covalent organic framework membranes for trace TMA sensing at room temperature, J. Colloid Interface Sci. 663 (2024) 262–269, https://doi.org/10.1016/j.jcis.2024.02.145.
[9] R. Nihal, M. Sharma, J.K. Sharma, Goswamy, synthesis and characterization of WO3–SnO2/rGO nanocomposite for Propan-2-ol sensing, Sensors International 3 (2022), https://doi.org/10.1016/j.sintl.2022.100172.
[10] X. Liu, S. Cheng, H. Liu, S. Hu, D. Zhang, H. Ning, A survey on gas sensing technology, Sensors (Switzerland) 12 (2012) 9635–9665, https://doi.org/10.3390/s120709635.
[11] K. Sivaperuman, A. Thomas, R. Thangavel, L. Thirumalaisamy, S. Palanivel, S. Pitchaimuthu, N. Ahsan, Y. Okada, Binary and ternary metal oxide semiconductor thin films for effective gas sensing applications: a comprehensive review and future prospects, Prog. Mater. Sci. 142 (2024) 101222, https://doi.org/10.1016/j.pmatsci.2023.101222.
[12] T. Ravikumar, L. Thirumalaisamy, A. Thomas, S. Nallakumar, S. Pandiaraj, M. Mr, A.N. Alodhayb, S. Pitchaimuthu, V. Dananjaya, C. Abeykoon, K. Sivaperuman, A. N. Grace, Impact of annealing temperature on the response and sensitivity of spinel ZnFe2O4 thin film to ammonia gas sensing at room temperature, Materials Today Chemistry 43 (2025) 102515, https://doi.org/10.1016/j.mtchem.2025.102515.
[13] R. Xavier, K. Sivaperuman, Review on the of physical vapor deposition on imminent chemiresistive metal oxide gas sensors and their future scope, Mater Today Commun 38 (2024) 107831, https://doi.org/10.1016/j.mtcomm.2023.107831.
[14] M. Epifani, Mechanistic insights into WO3 sensing and related perspectives, Sensors 22 (2022), https://doi.org/10.3390/s22062247.
[15] K. Aguir, A New Combined Transient Extraction Method Coupled with WO 3 Gas Sensors for Polluting Gases Classification to Cite this Version : HAL Id : HAL-03618788 a New Combined Transient Extraction Method Coupled with WO 3 Gas Sensors for Polluting Gases Classific, (2022).
[16] X. Chen, T. Liu, X.T. Yin, High response triethylamine gas sensor based on flaky W-doped MoO3, J. Ind. Eng. Chem. 129 (2024) 691–698, https://doi.org/10.1016/j.jiec.2023.09.027.
[17] S.J. Ippolito, A. Ponzoni, K. Kalantar-Zadeh, W. Wlodarski, E. Comini, G. Faglia, G. Sberveglieri, Layered WO3/ZnO/36° LiTaO3 SAW gas sensor sensitive towards ethanol vapour and humidity, Sens. Actuators B 117 (2006) 442–450, https://doi.org/10.1016/j.snb.2005.12.050.
[18] M. Balachandran, C. Thiyakarajan, R.H. Ramprasath, T. Logu, K. Sethuraman, Investigation on visible spectral response of spray coated Ni doped CuGaS2 thin films for photodetector application, Opt. Mater. 146 (2023) 114559, https://doi.org/10.1016/j.optmat.2023.114559.
[19] A. Mukherjee, Y. Rosenwaks, Recent advances in silicon fet devices for gas and volatile organic compound sensing, Chemosensors 9 (2021) 8–10, https://doi.org/10.3390/chemosensors9090260.
[20] Z. Lin, N. Li, Z. Chen, P. Fu, The effect of Ni doping concentration on the gas sensing properties of Ni doped SnO2, Sens. Actuators B 239 (2017) 501–510, https://doi.org/10.1016/j.snb.2016.08.053.
[21] S. Singkammo, A. Wisitsoraat, C. Sriprachuabwong, A. Tuantranont, S. Phanichphant, C. Liewhiran, Electrolytically exfoliated graphene-loaded flame-made Ni-doped SnO2 composite film for acetone sensing, ACS Appl. Mater. Interfaces 7 (2015) 3077–3092, https://doi.org/10.1021/acsami.5b00161.
[22] R. Sharma, K. Nihal, A.S. Bansal, M. Dhaliwal, J.K. Sharma, Goswamy, synthesis and characterization of WO3 based thin film electrode material for electrochromic device, Mater Today Proc 78 (2023) 895–899, https://doi.org/10.1016/j.matpr.2022.12.189.
[23] U.T. Nakate, Y.T. Yu, S. Park, High performance acetaldehyde gas sensor based on p-n heterojunction interface of NiO nanosheets and WO3 nanorods, Sens. Actuators B 344 (2021), https://doi.org/10.1016/j.snb.2021.130264.
[24] S. Nallakumar, L. Thirumalaisamy, S. Madhanagurusamy, S. Kalainathan, M. Usha Rani, Inverse and distorted Co2SnO4 cubic spinel thin films for dimethylamine detection at room temperature, New J. Chem. 47 (2023) 11110–11122, https://doi.org/10.1039/d3nj01409f.
[25] A.K. Mohamedkhair, Q.A. Drmosh, M. Qamar, Z.H. Yamani, Tuning structural properties of wo3 thin films for photoelectrocatalytic water oxidation, Catalysts 11 (2021) 1–16, https://doi.org/10.3390/catal11030381.
[26] H.T.T. Nguyen, T.H. Truong, T.D. Nguyen, V.T. Dang, T.V. Vu, S.T. Nguyen, X. P. Cu, T.T.O. Nguyen, Ni-doped WO3 flakes-based sensor for fast and selective detection of H2S, J. Mater. Sci. Mater. Electron. 31 (2020) 12783–12795, https://doi.org/10.1007/s10854-020-03830-9.
[27] A.K. Mishra, J. Willoughby, S.L. Estes, K.C. Kohler, K.S. Brinkman, Impact of morphology and oxygen vacancy content in Ni, Fe co-doped ceria for efficient electrocatalyst based water splitting, nanoscale, Advances 6 (2024) 4672–4682, https://doi.org/10.1039/d4na00500g.
[28] F. Mehmood, J. Iqbal, M. Ismail, A. Mehmood, Ni doped WO3 nanoplates: an excellent photocatalyst and novel nanomaterial for enhanced anticancer activities, J. Alloys Compd. 746 (2018) 729–738, https://doi.org/10.1016/j.jallcom.2018.01.409.
[29] W. Zhong, C. Yang, J. Wu, W. Xu, R. Zhao, H. Xiang, K. Shen, Q. Zhang, X. Li, Oxygen vacancies induced by charge compensation tailoring Ni-doped Co3O4 nanoflakes for efficient hydrogen evolution, Chem. Eng. J. 436 (2022) 134813, https://doi.org/10.1016/j.cej.2022.134813.
[30] U.T. Nakate, Y.T. Yu, S. Park, High performance acetaldehyde gas sensor based on p-n heterojunction interface of NiO nanosheets and WO3 nanorods, Sens. Actuators B 344 (2021), https://doi.org/10.1016/j.snb.2021.130264.

[31] X. Li, L. Fu, H. Karimi-Maleh, F. Chen, S. Zhao, Innovations in WO3 gas sensors: nanostructure engineering, functionalization, and future perspectives, Heliyon 10 (2024), https://doi.org/10.1016/j.heliyon.2024.e27740.
[32] M.S. Islam, K.R. Chowdhury, S.M. Hoque, A. Sharif, Cationic and oxygen defect modulation for tailoring the bandgap and room temperature ferromagnetism of CuO via multiple d-block cations, Mater. Adv. 5 (2024) 2946–2967, https://doi.org/10.1039/d3ma00987d.
[33] L.X. Lovisa, D.F. dos Santos, A.A.G. Santiago, M.D. Teodoro, M.R.D. Bomio, F. V. Motta, Synthesis of Pr3+−doped WO3 particles: correlation between photoluminescent and photocatalytic properties, RSC Adv. 13 (2023) 25738–25751, https://doi.org/10.1039/d3ra05136f.
[34] R. Xavier, L. Thirumalaisamy, S. Madhanagurusamy, K. Sivaperuman, Spray deposited pristine and Mo doped WO3 thin films for acetaldehyde gas sensing at room temperature, Ceram. Int. 50 (2024) 969–976, https://doi.org/10.1016/j.ceramint.2023.10.187.
[35] G. Mineo, M. Scuderi, E. Bruno, S. Mirabella, Engineering hexagonal/monoclinic WO3Phase junctions for improved electrochemical hydrogen evolution reaction, ACS Appl Energy Mater 5 (2022) 9702–9710, https://doi.org/10.1021/acsaem.2c01383.
[36] Z. Wang, M. Hu, Y. Wang, X. Liu, Y. Qin, Effect of solvothermal reaction temperature on the morphology of WO3 nanocrystals and their low-temperature NO2-sensing properties, J. Alloys Compd. 665 (2016) 173–179, https://doi.org/10.1016/j.jallcom.2016.01.056.
[37] S.S. Shendage, V.L. Patil, S.P. Patil, S.A. Vanalakar, J.L. Bhosale, J.H. Kim, P. S. Patil, NO 2 sensing properties of porous fibrous reticulated WO 3 thin films, J. Anal. Appl. Pyrolysis (2017), https://doi.org/10.1016/j.jaap.2017.05.006.
[38] T. Ravikumar, K. Sivaperuman, Fabrication of bare and cobalt-doped ZnFe2O4 thin film as NH3 gas sensor with enhanced response through UV-light illumination, Materials Today Chem. 38 (2024) 102049, https://doi.org/10.1016/j.mtchem.2024.102049.
[39] C.B. Rodella, D.H. Barrett, S.F. Moya, S.J.A. Figueroa, M.T.B. Pimenta, A.A. S. Curvelo, V. Teixeira Da Silva, Physical and chemical studies of tungsten carbide catalysts: effects of Ni promotion and sulphonated carbon, RSC Adv. 5 (2015) 23874–23885, https://doi.org/10.1039/c5ra03252k.
[40] K. Sasikumar, S. Thangabalu, M. Muthuramamoorthy, Ni-doped WO3 nanoparticles: an efficient dual-functional material for photocatalytic and antibacterial applications, Ceram. Int. 51 (2025) 21424–21440, https://doi.org/10.1016/j.ceramint.2025.02.302.
[41] N. Santhosh, M.U. Rani, Chemically sprayed pristine and cd 2+ incorporated Co2SnO4 thin films for low ppm level enhanced chemi - resistive behaviour towards dimethylamine detection at room temperature, J. Hazard. Mater. 469 (2024) 134041, https://doi.org/10.1016/j.jhazmat.2024.134041.
[42] K. Vijayan, L. Thirumalaisamy, S.P. Vijayachamundeeswari, Hierarchically Structured Sub-Band in Chalcopyrite Thin Film Solar Cell Device, (n.d.) 1–21.
[43] P. Srinivasan, A.J. Kulandaisamy, G.K. Mani, K.J. Babu, K. Tsuchiya, J.B. B. Rayappan, Development of an acetone sensor using nanostructured Co3O4 thin films for exhaled breath analysis, RSC Adv. 9 (2019) 30226–30239, https://doi.org/10.1039/c9ra04230j.
[44] K. Radha, B. Selvaraj, P. Srinivasan, A. Krishnakumar, J.B.B. Rayappan, K.J. Babu, Room-temperature acetaldehyde-sensing properties of SILAR-deposited ZnO thin films: role of tungsten doping, J. Mater. Sci. Mater. Electron. 32 (2021) 17700–17715, https://doi.org/10.1007/s10854-021-06307-5.
[45] Z. Cheng, S. Zhou, T. Chen, Y. Dong, W. Zhang, X. Chu, Acetic acid gas sensors based on Ni2+ doped ZnO nanorods prepared by using the solvothermal method, J. Semicond. 33 (2012) 1–6, https://doi.org/10.1088/1674-4926/33/11/112003.
[46] M.K. Deore, V.B. Gaikwad, R.L. Patil, N.K. Pawar, S.D. Shinde, G.H. Jain, Effect of Ni doping on gas sensing performance of ZnO thick film resistor, Sensors Transducers 122 (2010) 143.
[47] A.P. Rambu, L. Ursu, N. Iftimie, V. Nica, M. Dobromir, F. Iacomi, Study on Ni-doped ZnO films as gas sensors, Appl. Surf. Sci. 280 (2013) 598–604, https://doi.org/10.1016/j.apsusc.2013.05.033.
[48] R. Krishna, H. Cho, J. Yoon, Y. Yu, Fabrication of aggregated in 2 O 3 nanospheres for highly sensitive acetaldehyde gas sensors, J. Alloys Compd. 772 (2019) 834–842, https://doi.org/10.1016/j.jallcom.2018.09.183.
[49] J.M. Jun, Y.H. Park, C.S. Lee, Characteristics of a metal-loaded SnO2/WO3 thick film gas sensor for detecting acetaldehyde gas, Bull. Korean Chem. Soc. 32 (2011) 1865–1872, https://doi.org/10.5012/bkcs.2011.32.6.1865.
[50] Y. Shimizu, M. Egashira, Basic aspects and challenges of semiconductor gas sensors, MRS Bull. 24 (1999) 18–24, https://doi.org/10.1557/S0883769400052465.
[51] A. Giberti, M.C. Carotta, B. Fabbri, S. Gherardi, V. Guidi, C. Malagù, High-sensitivity detection of acetaldehyde, Sens. Actuators B 174 (2012) 402–405, https://doi.org/10.1016/j.snb.2012.08.016.
[52] W. Qu, W. Wlodarski, A thin-film sensing element for ozone, humidity and temperature, Sens. Actuators B 64 (2000) 42–48, https://doi.org/10.1016/S0925-4005(99)00481-5.
[53] H. Zhang, Y. Guo, F. Meng, Metal oxide semiconductor sensors for Triethylamine detection: sensing performance and improvements, Chemosensors 10 (2022), https://doi.org/10.3390/chemosensors10060231.